Quantitative trait locus mapping of osmotic stress response in the wheat pathogen *Zymoseptoria tritici*

Authors:

Jessica Stapley and Bruce A. McDonald

Plant Pathology Group, Institute of Integrative Biology, ETH Zurich, 8092 Zürich, Switzerland

Corresponding author: Jessica Stapley, Jessica.stapley@usys.ethz.ch

Abstract

Osmotic stress is a ubiquitous and potent stress for all living organisms. Fungal molecular responses to salt stress in well studied model yeast species highlighted the importance of the conserved HOG MAP kinase pathway. However, fewer studies have investigated the genetic basis of salt tolerance in filamentous fungi. The main aim of this study was to identify regions of the genome associated with tolerance to potassium chloride in the wheat pathogen *Zymoseptoria tritici.* A secondary aim was to identify candidate genes affecting salt tolerance within the most promising chromosomal regions. We achieved these aims with a quantitative trait locus (QTL) mapping study using offspring from two crosses grown in vitro in the presence or absence of osmotic stress imposed by 0.75M KCl. We identified significant QTL for most of the traits in both crosses. Several QTL overlapped with QTL identified in earlier studies for other traits and some QTL explained trait variation in both the control and salt stress environments. A significant QTL on chromosome 3 explained variation in colony radius at 8 days post inoculation (dpi) in the KCl environment as well as colony radius KCl tolerance at 8 dpi. The QTL peak had a high LOD and encompassed an interval containing only 36 genes. Six of these genes present promising candidates for functional analyses.

Keywords:
Salt stress; plant pathogen; fungi; *Mycosphaerella graminicola*, QTL

1. Introduction

Osmotic stress is a common and potent environmental stress that can limit growth and reproduction in many organisms. At the cellular level osmotic stress results in changes to the movement of water into or out of the cell through osmosis. To counteract osmotic stress, organisms need to accumulate compatible solutes (e.g. glycerol, erythritol, arabitol, mannitol and trehalose) – that can balance osmosis and provide turgor pressure (Araújo et al., 2020; Kogej et al., 2007). In fungal pathogens of plants, the pathogen may be exposed to a relatively high salt concentration (0.5M) within the plant (see Araújo et al., 2020) as well as experience changes in salt and osmolyte concentrations as plant tissues degrade (Jacob et al., 2015). The genes and pathways involved in responding to the resulting osmotic stresses may also affect plant-pathogen interactions and virulence. For example, turgor pressure which is mediated by changes in vacuole size and number is important in both plant tissue penetration and response to osmotic stress (Richards et al., 2010). Voltage-gated chloride channels, which are involved in the regulation of cell volume, also influence virulence in fungal pathogens of both plants and humans (Cañero and Roncero, 2008; Zhu and Williamson, 2003). Knowledge of the genetic basis of osmotic sensitivity in plant pathogens can thus provide important insights into the genetic basis of environmental stress responses as well as disease development.

The immediate effects of osmotic stress in fungi include stalled growth, changes in the recruitment of water, collapse of the cytoskeleton, altered plasma membranes and a reduction in glycerol transport (Duran et al., 2010; Hohmann, 2002). Longer-term adaptation to osmotic stress involves modifications of metabolism, plasma membranes, cell wall thickness and cell wall melanisation, as well as an accumulation of mycosporines (Hohmann, 2002; Kogej et al., 2007). Osmotic stress is also likely to activate many genes and pathways involved in the ‘general stress response’. For example, up to 10% of the genes that were differentially expressed under different individual stressors were shared across different osmotic stress treatments (Hohmann, 2002).

Although the key salt stress response pathways and genes have been identified and well characterized in model yeasts, studies in filamentous fungi could provide novel insights into the genes involved in responding to osmotic stress. The HOG pathway is an osmoresponsive

system and one of the most well-understood mitogen-activated protein (MAP) kinase pathways (Hohmann, 2002). In yeast, two genes are central components of this pathway – Pbs2 and Hog1p kinase. In plant pathogens, HOG signalling appears more complex than in yeast, although it is still poorly understood (Jacob et al., 2015). Several filamentous pathogenic fungi (including our model *Zymoseptoria tritici*) have multiple (up to 17) histidine kinases, whereas *S. cerevisiae* has only one (Sln1p) (Jacob et al., 2015). Several studies have identified transcription factors (TFs) involved in regulating the fungal response to salt stress, as well as other stressors - including temperature and fungicide stress. For example, in *Aspergillus oryzae*, GATA TFs were shown to be important in responding to salt and temperature stress (Jiang et al., 2021). In the causal agent of Fusarium head blight (*Fusarium graminearum*), the nutrient and stress factor 1 (NSf1) C_2H_2 zinc fingers protein plays an important role in salt stress response, sexual-asexual reproduction, vegetative growth, fungicide sensitivity and pathogenicity (Shi et al., 2021), and a Zn(2)-C6 fungal-type DNA-binding TF (Fss1) is required for sodium and lithium tolerance (Son et al., 2015). Cell wall melanisation also appears to confer benefits for osmotic stress tolerance. For example, cell wall melanisation in halotolerant fungi helps to maintain high concentrations of glycerol and contain the resulting turgor pressure by strengthening and preventing leakage through the cell wall (Kogej et al., 2007). These examples coming from a relatively small number of fungal species demonstrate how the molecular mechanisms of salt response can vary across taxa and illustrate that additional work is needed to understand how fungi adapt to salt stress.

To improve our understanding of osmotic stress response in fungi we performed a quantitative trait loci (QTL) mapping study using the wheat pathogen *Z. tritici* growing under salt stress. QTL studies have been instrumental in finding candidate genes for multiple traits in this widespread and damaging wheat pathogen, including melanisation (Lendenmann et al., 2014), fungicide sensitivity (Lendenmann et al., 2015), morphological switching (Francisco et al., 2022) and oxidative stress (Zhong et al., 2021), and enabled the cloning and functional validation of genes affecting virulence (Zhong et al., 2017; Meile et al. 2018), melanisation (Krishnan et al. 2018), and morphological switching (Francisco et al., 2022). QTL mapping identifies genomic regions that explain variation in a trait and that are likely to harbour genes responsible for creating variation in the trait. The aim of this study was to

98 identify large effect loci associated with tolerance to salt stress in *Z. tritici* and identify
99 plausible candidate genes within the most promising QTL intervals.
100
101 **2. Methods**
102 **2.1. QTL mapping crosses**
103 Parent and progeny isolates used in this study are from two crosses that were described
104 previously (Lendenmann et al., 2014). The original choice of strains for making crosses was
105 based upon a comprehensive phenotyping campaign of an international collection of 150
106 strains, including 30 strains from Switzerland (Zhan et al., 2005). In this original phenotyping
107 campaign, we measured seven traits for each strain, including in planta virulence and
108 pycnidia size and density, and growth rates in vitro under different temperatures and in the
109 presence of fungicides. Based on data from these seven traits, four Swiss strains were
110 selected to make the QTL mapping crosses that yielded 700 offspring over the two crosses.
111 The four parents have since been tested under other environmental stressors (e.g. reactive
112 oxygen (Zhong et al., 2021)) including KCl (0.25-1.0M). In the presence of 0.75M KCl the
113 parents differed in both growth and melanisation traits (Table S1). The crosses were made
114 by coinfecting wheat leaves with the parent strains, with the resulting ascospores collected
115 from infected leaves and grown in vitro. One cross was between ST99CH1A5 and
116 ST99CH1E4 (herein referred to as 1A5 and 1E4 respectively) and the other was between
117 ST99CH3D7 and ST99CH3D1 (herein referred to as 3D7 and 3D1 respectively).
118
119 **2.2. Genotyping**
120 SNP genotype data for the progeny were obtained from a RAD sequence dataset that was
121 previously produced in our lab (first described in (Lendenmann et al., 2014). In brief, the
122 genome was cut using the restriction enzyme *Pst*I and the libraries were sequenced on an
123 Illumina HiSeq2000 with paired-end sequencing. Complete genome sequences of the
124 parental strains (Croll et al., 2013)(NCBI Biosample: SRS383146 (ST99CH3D1), SRS383147
125 (ST99CH3D7), SRS383142 (ST99CH1A5), and SRS383143 (ST99CH1E4)) were used to SNP
126 genotype the parents and offspring.
127
128 RADseq processing and variant discovery is described in detail at
129 https://github.com/jessstapley/QTL-mapping-Z.-tritici. In brief, RADseq reads were trimmed

130 of adaptors and low-quality sequence using trimmomatic (v0.35). The RADseq reads were
131 mapped to a reference genome using bwa mem (v0.7.17). Reads from progeny of the
132 3D7x3D1 cross were mapped to the 3D7 reference genome and progeny from the 1A5x1E4
133 cross were mapped to the 1A5 reference genome. Variant calling was done using the GATK
134 Germline Short Variant Discovery pipeline, following their Best Practice recommendations
135 (https://gatk.broadinstitute.org/hc/en-us/sections/360007226651-Best-Practices-
136 Workflows). After this we applied the following filters: only biallelic SNPs, parents had
137 alternative alleles, <50% missing genotypes per marker, <50% missing genotypes per
138 individual, mean read depth >3 and <30, depth quality (QD)>5, mapping quality >40, minor
139 allele frequency >0.02 and <0.80, and SNPs in regions where the SNP density is >3 in 10bp
140 were removed.
141
142 **2.3. Generating linkage maps**
143 Linkage maps were made using R (R Core Team, 2020), R Studio (RStudio Team, 2020) and
144 the R package qtl (v1.48-1 (Broman et al., 2003)). As the order and base pair positions of the
145 markers were known from the reference genomes, we only needed to calculate the
146 recombination distance between markers to create the linkage map. Before map
147 construction, we removed putative clones. To do this we calculated genetic similarity using
148 the 'comparegeno' function and removed individuals with >99% shared genotypes (83
149 progeny were removed from the 1A5x1E4 cross, 74 progeny were removed from the
150 3D7x3D1 cross). The linkage map was constructed for each chromosome separately using
151 the 'estimatemap' function with method 'morgan'. Then we performed multiple rounds of
152 cleaning to remove error-prone markers that caused map inflation. First, we removed
153 markers that had an estimated recombination distance above the 99.9% quantile. Then
154 recombination rate was estimated again and we inspected the maps. In regions of the map
155 where there was evidence of map inflation and spurious double recombination events, we
156 visualised these regions in an Integrated Genome Viewer (IGV, https://igv.org) to look at the
157 mapping alignments. Markers were removed from regions with poor alignments and
158 evidence of mismapping. A summary of the two linkage maps is provided in Supplementary
159 Material S1 and the complete maps are available at (https://github.com/jessstapley/QTL-
160 mapping-Z.-tritici). After applying all of these filters, the average marker spacing was 1217
161 bp (0.19 cM) and 529 bp (0.14 cM) for the 1A5x1E4 and 3D7x3D1 crosses, respectively.

162

163 **2.4. Phenotyping**

164 We compared colony growth and melanisation in a control environment and in the
165 presence of potassium chloride (KCl) to simulate a salt stress environment. Potassium
166 chloride (KCl) has been used extensively in the study of stress responses in fungi because it
167 is environmentally ubiquitous and lacks the toxic effects of Na^+ (Araújo et al., 2020;
168 Hohmann, 2002). Only non-clonal offspring strains were phenotyped (for 1A5x1E4 n= 259
169 strains; for 3D7x3D1 n=265 strains). The basic protocols for isolate recovery from -80^{0}C
170 storage, growth in vitro and the measurements of colony size and colony melanisation were
171 described previously (Zhong et al., 2021). In brief, Petri dishes containing Difco potato
172 dextrose agar (PDA) were inoculated with 200µl of a spore solution (concentration 200
173 spores/ml) and grown at 18^{0}C for 8 and 12 days. In the salt stress environment, a sterile
174 potassium chloride solution was added to the cooled and sterilized PDA to make a final
175 concentration of 0.75M. Three replicates were grown in both the control and salt (KCl)
176 environments.

177

178 Two traits were measured; colony area and colony grey value, using automated image
179 analysis as described previously (Lendenmann et al., 2014; Zhong et al., 2021). Grey value
180 was measured on a scale of 0-255, where darker, more melanised colonies have lower
181 values (0 = black, 255 = white). Mean colony area (mm^2) and grey value were calculated
182 from measurements of multiple colonies on each plate and then the mean was calculated
183 across the three replicate plates to obtain a final mean colony area and mean grey value for
184 each strain in the two environments. Colony area was converted to colony radius by dividing
185 by π and taking the square root of this value. Measurements were taken at 8- and 12-days
186 post inoculation (dpi). For the analysis we used three different types of data; (1) time
187 point/age: the colony radius and grey value at 8 and 12 dpi; (2) daily rate measurements:
188 the change in colony radius or grey value between 8 and 12 dpi (i.e. the difference in colony
189 radius between 8 and 12 dpi/difference in days); and (3) KCl tolerance measurements: the
190 ratio of a measurement (colony radius, grey value, growth rate or melanisation rate)
191 between the KCl environment and the control environment (i.e. colony radius KCl tolerance
192 at 8dpi = colony radius at 8 dpi in the KCl environment/colony radius at 8 dpi in the control
193 environment, or growth rate KCl tolerance = growth rate in the KCl environment/growth

194 rate in the control environment). For the KCl tolerance measurements, values >1 indicate
195 that for that trait an isolate is more tolerant to KCl (higher value under salt stress), and
196 values <1 indicate that for that trait measured an isolate is more sensitive to KCl. In total
197 there were 18 traits (Table 1).
198
199 **2.5. QTL mapping**
200 QTL mapping was performed using the R (v 3.6.0) package 'qtl2' (v2_0.24) as described in
201 detail on github (https://github.com/jessstapley/QTL-mapping-Z.-tritici). We scanned the
202 genome for a single QTL per chromosome with the '*scan1*' function using a linear mixed
203 effect model, and we controlled for the relatedness of individuals (i.e. we included a
204 random polygenic effect) by fitting the kinship matrix as a random effect. Models that take
205 into account the genetic covariance between individuals can reduce the false discovery rate
206 in QTL scans and outperform models that do not include this information in the model
207 (Malosetti et al., 2011). The significance threshold for a QTL peak was determined by
208 permutation tests (n=1000) and we calculated a Bayes Credible Interval (95%) to identify the
209 interval size around the QTL peak. We used custom R scripts to extract a list of the genes
210 within the interval from the annotation (gff) files of each reference genome. The putative
211 encoded function of each gene was determined in previous analyses (for 1A5 see
212 (Plissonneau et al., 2018), for 3D7 see (Plissonneau et al., 2016)). The annotations were
213 obtained using Interproscan (https://www.ebi.ac.uk/interpro/) against multiple protein
214 databases and then screened using multiple methods (e.g. 8ignal
215 https://services.healthtech.dtu.dk/service.php?SignalP-5.0, Phobius
216 https://phobius.sbc.su.se/) to determine if the encoded proteins contained likely signal
217 peptides or secreted domains. The putative effect of a SNP in the coding sequence was
218 determined using SNPeff (http://pcingola.github.io/SnpEff/).
219
220 **2.6. Identifying putative candidate genes in the 3D7x3D1 cross**
221 Genes within a single QTL interval on chromosome 3 were further investigated to identify
222 the most likely candidate genes responsible for the phenotype. We identified the
223 orthologous genes in the 3D1 parent using an analysis performed across the genomes of 19
224 reference strains (Badet et al., 2020). We inspected the alignments in the region of interest

225 in IGV. We also blasted the 3D1 gene sequences (including ±200bp flanking regions) against
226 the 3D7 genome to calculate sequence similarity and identify indels.
227
228 **2.7. RNAseq data analysis**
229 We analysed RNAseq data that was previously created for the four parental strains during
230 infection of the susceptible wheat cultivar Drifter (Palma-Guerrero et al., 2017) as well as
231 cultures grown in vitro on two types of liquid media (yeast sucrose broth (YSB): yeast extract
232 10 g/L and sucrose 10 g/L, pH 6.8; and carbon-depleted minimal medium (MM), pH 5.8
233 (Francisco et al., 2019)). The raw sequence reads were downloaded from the Short Read
234 Archive (SRA, https://www.ncbi.nlm.nih.gov/sra, Bioproject: *invitro* SRP152081, *invivo*
235 SRP077418). RNAseq data processing and analysis is described in detail at github
236 (https://github.com/jessstapley/QTL-mapping-Z.-tritici). In brief, reads were trimmed and
237 then mapped to one of two reference genomes (reads from 3D1 and 3D7 were mapped to
238 the 3D7 reference genome while reads from 1E4 and 1A5 were mapped to the 1A5
239 reference genome). Then the number of reads mapping to each gene was counted using
240 R::Rsubread (Liao et al., 2019) and we tested for differential gene expression between
241 strains, 3D7 versus 3D1 and 1A5 versus 1E4, using R::EdgeR (Robinson et al., 2010).
242
243 **3. Results**
244 **3.1. Effect of KCl on growth and melanisation**
245 A total of 158,480 and 120,059 colonies from the 1A5x1E4 and 3D7x3D1 crosses,
246 respectively, were phenotyped (see Table S2 for details). Differences in growth and
247 melanisation between salt stress and control environments, and growth rate KCl tolerance
248 of and melanisation rate KCl tolerance can be seen in Figure 1. We used paired Wilcoxon
249 tests to compare mean trait values between the control and KCl treatments (Table S2). In
250 the presence of KCl, colony radius was smaller at 8 and 12 dpi in both crosses, and the
251 growth rate was reduced in the 3D7x3D1 cross, but not in the 1A5x1E4 cross, suggesting
252 that isolates from the 3D7x3D1 cross were more sensitive to KCl (Figure 1, Table S2). This is
253 consistent with the greater growth rate tolerance in the 1A5x1E4 cross compared to the
254 3D7x3D1 cross ($F_{(1,487)} = 9.19$, p=0.002, growth rate KCl tolerance: 1A5x1E4 = 1.04, 3D7x3D1
255 = 0.96). In the KCl environment we observed less melanisation at both time points and a
256 similar reduced accumulation of melanin over time (melanisation rate) in both crosses

257 (Figure 1, Table S2, $F_{(1,486)}$ = 2.85, p=0.09, melanisation rate KCl tolerance: 1A5x1E4 = 0.196,
258 3D7x3D1 = 0.149).
259
260 **3.2. Correlations between traits**
261 All pairwise correlations (Pearson, non-parametric) between independent measurements
262 are provided in Tables S3 and S4. Excluding traits that are statistically or functionally
263 coupled, which includes: correlations between two time points of the same trait (e.g. colony
264 radius at 8 dpi and 12 dpi in the control), correlations between a rate and the corresponding
265 time point measurements (e.g. grey value at 12 dpi and melanisation rate in the control), or
266 correlations between rates and KCl tolerance measurements, we identified many
267 correlations between independent measurements (Table S3 and S4). Notably, growth rate in
268 the control environment was correlated with growth rate in the KCl environment in both
269 crosses (r(1A5x1E4) = 0.63 and r(3D7x3D1) = 0.62, Figure S2) – thus isolates that grow faster
270 in a benign environment also grow faster in the presence of salt stress, i.e. they have a
271 higher intrinsic growth rate. Melanisation rates showed a similar trend in 1A5x1E4 – isolates
272 that had higher melanisation rates in the benign environment also had higher melanisation
273 rates under KCl stress (Table S4, r = 0.19), but this was not observed in the 3D7x3D1 cross
274 (Table S3, r = 0.07, Figure S2).
275
276 We were particularly interested in the relationship between KCl tolerance and melanisation,
277 as melanin can help protect cells from osmotic stress. In both crosses, the mean grey value
278 in the control environment at 12 dpi was negatively correlated with growth rate KCl
279 tolerance (Tables S2 and S4, 1A5x1E4 r = -0.26 and 3D7x3D1 r = -0.43, Figure S2). The
280 relationship at 8 dpi was also negative in both crosses, but not significant in the 3D7x3D1
281 cross (Tables S3 and S4, 1A5x1E4 r = -0.44 and 3D7x31 r = -0.12, Figure S2). As lower mean
282 grey values correspond to higher amounts of melanin, these correlations indicate that
283 isolates that produce more melanin in a benign environment have a growth rate that is
284 more tolerant to KCl stress, although this relationship was not significant at 8 dpi in the
285 3D7x3D1 cross.
286
287 **3.3. QTL results**

288 We identified at least one significant QTL for all but three traits (melanisation rate and mean
289 grey value at 12 dpi in the KCl environment, and melanisation rate KCl tolerance at 12dpi) in
290 the 1A5x1E4 cross and all but one trait (melanisation rate KCl tolerance) in the 3D7x3D1
291 cross (Table 1). In general, the traits lacking significant QTL had relatively low heritability
292 (Table 1) and thus the power to detect a QTL for those traits was relatively low. All QTL
293 positions, interval sizes and numbers of genes within the interval are presented in Tables 2
294 and 3. Overlapping QTL were grouped and given a unique QTL identifier. Examples of how
295 traits measured in different environments can have overlapping QTL intervals are shown in
296 Figure 2. The QTL No. 4, 9 and 11 are each regions of the genome that explain variation in
297 growth rate in both the KCl and control environments. As expected, traits that were highly
298 correlated and/or statistically coupled often had a QTL peak at the same, or overlapping
299 positions (e.g. the 1A5x1E4 grey values in the control environment at 8 dpi and 12 dpi
300 mapped to the same position on Chr 2: 1438934bp; the 3D7x3D1 QTL for colony radius at 12
301 dpi and growth rate in the control environment mapped to Chr 8: 1100862bp). LOD plots for
302 all traits listed in Tables 2 and 3 are provided in the Supplementary Information S3 and S4.
303 In Figures 2 and 3 we provide example plots for only four traits (growth rate in KCl, growth
304 rate in the control, melanisation rate in KCl and melanisation rate in the control) for the two
305 crosses.
306
307 **3.4. QTL shared across environments, traits, and time points**
308 Several QTL were shared amongst benign and salt-stress environments, across time points
309 and traits. Only one of these shared QTL is novel to this study, the other shared QTL were
310 found in earlier studies investigating different stressors. The single novel QTL shared
311 between benign and salt-stress environments was found in the 3D7x3D1 cross on Chr 8
312 (1100.86-1221.33 Kb, QTL No. 9, Figure 2) and explained variation in seven traits including
313 growth in the control and KCl environments, as well as mean grey value in the control
314 environment and grey value KCl tolerance at 8 dpi (Figure 2, Table 2).
315
316 Of the QTL shared across benign and KCl environments that were identified here and found
317 in earlier studies using different stresses (e.g. cold, fungicide), the most striking – in terms of
318 the number of traits and the magnitude of the LODs, was the QTL on Chr 11 between
319 507.36-658.11 Kb (QTL No. 12) in the 3D7x3D1 cross. This QTL explained variation in 11 of

320 the 18 traits, and in both environments (Table 2). This QTL was identified previously and was
321 found to explain variation in growth, fungicide sensitivity and melanisation in this cross
322 (Lendenmann et al., 2015, 2014). The next largest, in terms of number of traits, was a QTL in
323 the 1A5x1E4 cross on Chr 8 between 89.573- 346.224 Kb (QTL No. 13) that explained
324 variation in growth rate, colony radius and grey value in both control and KCl environments
325 (Figure 3, Table 3). This QTL on Chr 8 was also found to explain variation in response to
326 oxidative stress (Zhong et al., 2021). Another notable QTL in terms of high LOD (>10) was on
327 Chr 10 (749.521– 1302.645 Kb, QTL No. 10) in the 3D7x3D1 cross, which explained variation
328 in melanisation rate and colony radius in the control environment (Table 2). This QTL was
329 previously found to explain variation in growth-related traits at 10^0C (Lendenmann et al.,
330 2014) and under oxidative stress (Zhong et al., 2021).
331
332 **3.5. A unique QTL associated with the KCl environment**
333 Several novel QTL that were unique to the KCl environment were also found (Table 2, 3). In
334 the 3D7x3D1 cross, two QTL were found for traits related to colony radius: the first on Chr 3
335 (QTL No. 3) explained variation in colony radius at 8 dpi and colony radius KCl tolerance at 8
336 and 12 dpi; and the second on Chr 4 (QTL No. 5) explained variation in colony radius at 8 dpi
337 and colony radius KCl tolerance at 8 dpi. For melanin-related traits, four QTL were found in
338 the 3D7x3D1 cross: the first on Chr 1 (QTL No. 1) explained variation in three traits
339 (melanisation rate, melanisation rate KCl tolerance and grey value at 12 dpi); the second on
340 Chr 2 (QTL No. 2) explained variation in grey value at 12 dpi; the third on Chr 6 (QTL No. 6)
341 explained variation in melanisation rate; and the fourth on Chr 8 (QTL No. 8) explained
342 variation in grey value at 8 dpi. In the 1A5x1E4 cross a total of five QTL related to colony
343 radius in KCl were found. The first three were on Chr 1: QTL No. 2 explained variation in
344 colony radius KCl tolerance at 12 dpi; QTL No. 3 explained variation in growth rate KCl
345 tolerance; and QTL No. 4 explained variation in colony radius at 12 dpi. The fourth unique
346 KCl environment QTL was on Chr 5 (QTL No. 10) and explained variation in growth rate KCl
347 tolerance; the fifth on Chr 6 (QTL No. 11) explained variation in radius at 8 dpi
348
349 To identify candidate genes associated with KCl stress, we focused attention on novel QTL
350 with a high LOD (>10), relatively narrow intervals, and that explained a relatively high
351 proportion of the variation for a KCl-associated trait. Only QTL No. 3 in the 3D7x3D1 cross

352 met these requirements (Table 2). This QTL had a high LOD (>10) for colony radius at 8 dpi in
353 the KCl environment and colony radius KCl tolerance at 8 dpi. The LOD peaked at 22.8 at
354 chromosome position 737773 bp. This QTL explained 33% of the phenotypic variance in
355 colony radius at 8 dpi and 23% of the variance in colony radius KCl tolerance at 8 dpi.
356 Isolates with the non-reference allele at all markers within the interval had smaller colonies
357 (F=113.1, df=1,233, p=<0.001, Figure 4c) and less colony radius KCl tolerance at 8 dpi
358 (F=113.1, df=1,233, p=<0.001). The Bayes confidence interval for the QTL for colony radius
359 in KCl at 8 dpi spanned 149.29 Kb and contained 94 SNPs and 36 genes (Table 2, Figure 4b).
360 For this interval we present data on the genes in the reference genome (3D7), the
361 orthologous genes in 3D1, the gene sequence similarity (including ±200bp of flanking
362 regions) between the parents, the gene's putative encoded function (PFAM database) and if
363 there is any evidence of differential gene expression between the parents across all
364 available datasets (Table 4 and see Table S5 for full details).
365
366 **3.6. Candidate genes within QTL No. 3 in 3D7x3D1**
367 Several genes had SNP variation predicted to have a high impact based on SNPEff analysis
368 (Table S6, *ZT3D7_G3622*, *ZT3D7_G3623*, *ZT3D7_G3624, ZT3D7_G3632, ZT3D7_G3633,*
369 *ZT3D7_G3635, ZT3D7_G3649*). A transposable element (6927bp) was found within 200bp of
370 *ZT3D7_G3623*, and one gene, *ZT3D7_G3649* is a singleton – with no orthologue present in
371 any of the other 18 *Z. tritici* reference genome sequences (Table S5). Based on predicted
372 protein function, and sequence and gene expression variation between the parents, we
373 consider six genes to be the most promising candidates for further analyses: *ZT3D7_G3622*,
374 *ZT3D7_G3635*, *ZT3D7_G3637*, *ZT3D7_G3639*, *ZT3D7_G3655* and *ZT3D7_G3658* (this order
375 reflects their relative positions on chromosome 3).
376
377 *ZT3D7_G3622* has a loss of function SNP (Chr 3:598092) in 3D1 that is predicted to cause a
378 loss of a predicted start codon. The gene contains a single exon, encodes a protein length of
379 550 amino acids (aa) and is predicted to contain a fungal-specific transcription factor
380 domain and Zn(2)-C6 fungal-type DNA-binding domain (Table 4). The orthologue in the 3D1
381 genome is *ZT3D1_G3567*. It encodes a longer protein (722 aa) and has two exons, the first
382 exon's product encodes a Zn(2)-C6 fungal-type DNA-binding domain and the second exon's
383 product is the same as that of *ZT3D7_G3622*. The predicted protein in 3D1 is the same as

384 the orthologue In IPO323 (*Mycgr3T108446*). Although we do have reads mapping to this
385 region, and when grown in vitro on MM this gene is downregulated in 3D1 compared to 3D7
386 (Table S5), our RNA sequence data does not clearly support gene models in either 3D1 or
387 3D7, there are no clear exon/intron boundaries. This suggests that the annotation of this
388 gene may require manual curation.
389
390 *ZT3D7_G3635* has a high impact SNP variant (Chr 3:681906) that is predicted to cause a
391 frameshift. The gene has 6 exons in 3D7 and encodes a protein length of 1078 aa. Based on
392 INTERPROSCAN and Ensemble Fungi, the protein has multiple predicted domains; the
393 largest is a protein kinase domain. The protein also contains a Serine/threonine-protein
394 kinase active site and the molecular function of the first GO term (GO:0004674) is protein
395 serine/threonine kinase activity – suggesting that this gene is likely to be involved in osmotic
396 stress response (Hohmann, 2002). The RNA sequence data supports the gene model. The
397 orthologue in 3D1 is *ZT3D1_G3580*, which has 3 exons and multiple predicted domains that
398 do not differ from those predicted for *ZT3D7_G3635*. The gene is up-regulated in vitro on
399 YSB and down-regulated in planta at 28d in 3D1 compared to 3D7 (Table S5).
400
401 *ZT3D7_G3637* has one exon, encodes a protein length of 1285 aa, and includes multiple
402 predicted domains including a DEAD/DEAH box helicase, which is involved in plant
403 responses to osmotic stress (Nguyen et al., 2018). The orthologue in 3D1 (*ZT3D1_G3583*)
404 encodes a similar protein as *ZT3D7_G3637* – has the same length and has the same
405 predicted domains. There are no high impact SNPs between the parents, but several
406 moderate and low impact variants were identified (Table S6). The RNA sequence data
407 supports the annotation, and the gene is down regulated in 3D1 in both YSB and MM (Table
408 S5).
409
410 *ZT3D7_G3639* has 4 exons in 3D7. The gene sequence similarity between 3D7 and 3D1 is
411 98.66% and there is an 8bp intronic deletion in 3D1. This gene belongs to the Major
412 Facilitator Superfamily (MFS) and encodes a protein length of 512 aa. According to the
413 Phobius analysis, the gene contains 12 transmembrane segments (Table S5). Proteins with
414 transmembrane activity and transmembrane segments are likely to play an important role
415 in sensing and regulating osmotic stress (Hohmann, 2002). The orthologue in 3D1 is

416 *ZT3D1_G3580*, which has the same number of exons, encodes the same protein length and
417 has the same predicted function. The RNA sequence data supports the gene model, and the
418 differential expression analysis found the gene is downregulated in planta at 12 and 14 days
419 in 3D1 compared to 3D7 (Table S5).
420
421 *ZT3D7_G3655* has one exon and encodes a protein length of 848 aa. The gene contains 10
422 transmembrane segments (Table S5) and encodes a voltage-gated chloride channel domain
423 – thus it is likely to be involved in osmotic stress responses. The gene sequence between the
424 parents is almost identical, but there is one moderate effect SNP within the gene (Table S6).
425 When grown in vitro on MM this gene is upregulated in 3D1 compared to 3D7. The RNA
426 sequence data supports the gene model annotation.
427
428 *ZT3D7_G3658* has four exons and encodes a protein length of 614 aa. Its orthologue in 3D1
429 (*ZT3D1_G3604*) has three exons and encodes 572 aa. The gene encodes a vacuolar protein
430 sorting-associated protein 17, Vps17. Vacuoles play an important role in osmotic stress
431 responses: their fission and fusion enable cells to maintain turgor pressure and regulate cell
432 volume (Richards et al., 2010). Comparison of the 3D1 gene sequence to the 3D1 genome
433 using BLAST revealed that the 3D7 gene sequence was identical, but the 3D1 orthologue
434 annotation is shorter and has only three exons. Our RNA sequence data supports the 3D1
435 annotation with only 3 exons, as there were no RNA sequence reads mapping to exon 1 of
436 the *ZT3D7_G36580*. This gene was downregulated in vitro in both MM and YSB in 3D1
437 compared to 3D7.
438
439 **4. Discussion**
440 We were able to map major effect loci affecting colony growth and melanisation in the
441 presence of potassium chloride in both crosses. We focussed on QTL that were unique to
442 the KCl environment to identify candidate genes that are specific to osmotic stress – as
443 opposed to finding genes that may be more generally related to intrinsic growth or melanin
444 production. A QTL on Chr 3 in the 3D7x3D1 cross was the most promising for identifying
445 genes specifically associated with KCl stress. We highlighted the six most promising
446 candidate genes in this QTL based on their predicted encoded functions, sequence similarity
447 and transcriptional profiles. We also identified several QTL shared across environments and

448 confirmed that several previously identified QTL, which explained variation in growth and
449 melanisation across different environmental stressors (Table 2 and 3, e.g. 3D7x3D1 Chr 11
450 and 1A5x1E4 Chr 8), also explained trait variation in the presence of osmotic stress.
451
452 **4.1. Effect of KCl on colonies**
453 In the presence of potassium chloride at 0.75M, colonies were typically smaller and less
454 melanised compared to the control environment (Figure 1, Table S2). A reduction in colony
455 radius in the KCl environment supports our hypothesis that this environment was stressful
456 to *Z. tritici*. Our results suggest that growth rate in the 1A5x1E4 cross was less affected by
457 KCl-induced osmotic stress, as mean growth rate was not reduced in the KCl environment,
458 compared to the 3D7x3D1 cross that exhibited a significantly reduced growth rate (Table
459 S2). However, we note that the overall difference in growth rate in the 3D7x3D1 progeny
460 between the control and KCl environments was relatively small (~6% reduction in growth,
461 Table S2).
462
463 When experiencing osmotic stress, an increase in melanin is thought to protect cells by
464 strengthening the fungal cell wall, but a reduced metabolic capacity under stress may limit
465 the ability of a cell to produce melanin. The mean colony grey values were higher, indicative
466 of lower levels of melanin, for strains grown in the KCl environment (Table S2). This suggests
467 that the *Z. tritici* response to osmotic stress did not involve an increased production of
468 melanin to protect the cells as was observed in halotolerant species (Kogej et al., 2007). We
469 did observe however, that isolates that were more melanised in the benign control
470 environment (lower Grey Value) were more tolerant to salt stress (Figure S2) – their growth
471 rates were higher and their reductions in melanisation were lower compared to isolates that
472 were less melanised in the control environment (Table S3, S4). This suggests that strains
473 having a greater intrinsic capacity to become melanised are more tolerant to salt stress.
474
475 **4.2. Shared QTL**
476 Some QTL that explained variation in growth and melanisation in the stressful environment
477 overlapped with QTL for trait variation in the control environment. Prominent examples
478 include the Chr 11 QTL No. 11 in the 3D7x3D1 cross and the Chr 8 QTL No. 13 in the
479 1A5x1E4 cross. These genomic regions may harbour genes that affect intrinsic growth of

480 colonies under a wide range of environments and/or genes with pleiotropic effects. Many of
481 the QTL shared across environments were identified in earlier experiments and discussed
482 previously (Lendenmann et al., 2015; Zhong et al., 2021). The QTL No. 11 was shown to be
483 due to differential expression of the *Zmr1* gene encoding a transcription factor that
484 regulates synthesis of DHN melanin in *Z. tritici* (Krishnan et al. 2018). *Zmr1* was shown to
485 have pleiotropic effects on melanin production, colony growth rates and fungicide
486 resistance (Krishnan et al. 2018).
487
488 **4.3. QTL uniquely associated with the KCl environment**
489 This QTL analysis enabled us to identity large effect loci that explain variation in traits under
490 KCl stress. Among the QTL uniquely associated with KCl stress, most had moderate LODs
491 with each QTL explaining only a small proportion of the phenotypic variance (3D7x3D1
492 maximum = 0.10, 1A5x1E4 maximum = 0.11). The exception was QTL No. 3 in the 3D7x3D1
493 cross, which explained up to 33% of the phenotypic variance. This QTL on chromosome 3
494 was associated with differences in colony radius at 8 dpi and colony radius KCl tolerance at 8
495 and 12 dpi. We targeted this QTL for further investigation, seeking to identify genes
496 specifically associated with KCl tolerance. It is interesting to note that no LOD peak was
497 detected for colony radius at 12 dpi, even though colony radius at 12 dpi was correlated
498 with colony radius at 8 dpi (Table S3, correlation = 0.58, $p<0.001$). As growth rate is based
499 on the change in colony radius between 8 and 12 dpi, we might expect growth rate in KCl to
500 share the QTL for colony radius at 8 dpi. To better understand why growth rate does not
501 share this QTL, we examined the trait correlations. Growth rate is highly correlated with
502 colony radius at 12 dpi (0.93) and less strongly correlated with colony radius at 8 dpi (0.26)
503 (Table S3). There is less variation in colony radius at 8 dpi, thus colony radius at 12 dpi has a
504 greater impact on the growth rate. The QTL No. 3 also explained variation in colony radius
505 KCl tolerance at 8 and 12 dpi, although the association with this trait at 12 dpi explained
506 relatively little phenotypic variation (0.08). Thus, the QTL peak is more strongly associated
507 with colony radius and colony radius KCl tolerance at an earlier stage of colony growth. A
508 similar pattern was observed in the chromosome 11 QTL associated with melanisation
509 (Krishnan et al., 2018; Lendenmann et al., 2014), with the QTL LOD score very high in the
510 younger colonies and decreasing as colonies aged. After cloning and characterizing the *Zmr1*
511 gene and its functions, this pattern could be explained based on the finding that the

512 difference in *Zmr1* expression (and the resulting difference in melanisation) was significantly
513 higher in younger colonies than in older colonies (Krishnan et al., 2018). We hypothesize
514 that QTL no. 3 associated with KCl tolerance is underpinned by a similar mechanism that is
515 specific to the earlier stage of colony growth.
516
517 **4.4. Candidate genes in the QTL for colony radius and colony radius KCl tolerance at 8 dpi**
518 **in the 3D7x3D1 cross**
519 Among the 36 genes found in the interval spanning this QTL No. 3, we consider six genes to
520 be the most promising candidates to be involved in sensing and responding to salt stress
521 and responsible for this QTL. Below we consider each in turn in the order of their relative
522 positions on chromosome 3.
523
524 The first candidate gene, *ZT3D7_G3622*, is predicted to encode a fungal-specific
525 transcription factor. The orthologue in the IPO323 reference genome (assembly MYCGR
526 v2.0) is *Mycgr3T108446* and it has 21 paralogs. Transcription factors (TFs) regulate gene
527 expression and are important regulators of molecular responses to environmental stimuli
528 (e.g. Hohmann, 2002; Shi et al., 2021), making this gene a good candidate. The *Zmr1* gene
529 identified in this same cross and shown to be responsible for differences in melanisation,
530 with greater effects in younger colonies, is a transcription factor (Krishnan et al. 2018). The
531 SNP variant in 3D1 (Chr 3:598092) is predicted to cause a loss of the start codon that is likely
532 to cause a loss of function. In *F. graminearum,* mutants lacking a similar TF (called *Fss1*)
533 were sensitive to high sodium and lithium, but they were not sensitive to elevated
534 potassium (Son et al., 2015).
535
536 The second candidate, *ZT3D7_G3635* is predicted to encode a serine/threonine-protein
537 kinase active site, which is known to regulate MAP kinases (Hohmann, 2002; Li et al., 2019).
538 A SNP variant found in the 3D1 allele is predicted to cause a frameshift that is likely to cause
539 a loss of function. The ortholog in the IPO323 genome is *Mycgr3G56270* and it has one
540 paralog in the reference genome. A serine/threonine kinase from *Aspergillus flavus*,
541 *AflSte20*, was recently functionally validated using a knockout mutant. This study showed
542 that the knockout had higher sensitivity to osmotic stress compared to the wild type (Li et

543 al., 2019), confirming the role of this serine/threonine-protein kinase in osmotic stress
544 response in a different fungal plant pathogen.
545
546 The third candidate, *ZT3D7_G3637* is predicted to encode a DEAD/DEAH box helicase
547 domain. The reference genome orthologue is *Mycgr3G99415* and it has 6 paralogs. The
548 DEAD – box helicases are the largest RNA helicase (RH) subfamily. In plants they play
549 multiple functional roles and are important in stress responses (Pandey et al., 2020). For
550 example, in *Arabidopsis thaliana AtRH17* is involved in salt-stress tolerance (Nguyen et al.,
551 2018), in rice *OsABP* is upregulated in response to salt (Macovei et al., 2012) and in barley
552 HvD1 accumulated in salt- and cold-stressed plants (Nakamura et al., 2004). In wheat, the
553 DEAD-box helicase *TaRH1* that was first identified as a component of the defence response
554 to stripe rust (*Puccinia striiformis f*. sp. *tritici*) was also found to be involved in plant
555 response to multiple stressors, including salt stress (Zhang et al., 2014). SNP variation found
556 between the parents was predicted to have only moderate effects, no high impact SNPs
557 were detected. We chose this gene as a promising candidate based mainly on its known
558 associations with salt stress in plants and the significant differences in expression found
559 between 3D1 and 3D7 while growing in vitro.
560
561 A gene encoding a Major Facilitator Superfamily (MFS) domain, *ZT3D7_G3639* is the fourth
562 candidate we highlight. The reference genome orthologue is *Mycgr3G85019* and it has 58
563 paralogs. MFS transporters facilitate the movement of small solutes across cell membranes
564 in response to chemiosmotic gradients – making them likely to play an important role in
565 sensing and regulating osmotic stress (Hohmann, 2002). We chose this gene as a promising
566 candidate based mainly on its known functions and associations with multiple stressors
567 including fungicides (Dos Santos et al., 2014; Omrane et al., 2015).
568

569 The fifth highlighted gene is *ZT3D7_G3655* that encodes a voltage gated chloride channel
570 domain and membrane transport domains. The reference genome orthologue is
571 *Mycgr3T20761* and there are three paralogues in the IPO323 reference genome. Chloride
572 channels are important in animal cell volume regulation (Jentsch et al., 2002), fungal
573 oxidative stress response (Oddon et al., 2007), fungal pathogen virulence (Cañero and

574 Roncero, 2008; Zhu and Williamson, 2003) and plant immunity (Guo et al., 2014). The role of
575 chloride channels in response to salt stress is well established in animals (Jentsch et al.,
576 2002), and to a lesser degree in plants (Barbier-Brygoo et al., 2011), but less is known from
577 fungi. For one of the better-known families of chloride channels, the CLC family, a single
578 gene (*GEF1*) has been identified in yeast. In two pathogenic fungi (*Cryptococcus neoformans*
579 and *Fusarium oxysporum*) – the GEF1 homologue has been shown to influence virulence
580 (Cañero and Roncero, 2008; Zhu and Williamson, 2003). The gene sequence between the
581 parents is highly conserved, however gene expression differences were observed in minimal
582 media, so differences may exist in the regulatory sequence.

583

584 The final candidate we highlight is *ZT3D7_G3658*, which encodes a Vacuolar associated
585 protein 17, *Vps17*. The orthologous gene in the reference genome is *Mycgr3T108464* and
586 there are six paralogues. Comparing the DNA sequence of this gene against the 3D1 genome
587 revealed an identical sequence, but the annotation of the 3D7 and 3D1 differs – the 3D1
588 orthologue protein length is shorter and the gene has one fewer exons. Our RNA sequence
589 data suggests that the *ZT3D7_G3658* annotation may be incorrect - there were no reads
590 mapping to the first, small exon of this gene. This suggests that the annotation of this gene
591 may need manual curation before conducting further analyses. The gene was
592 downregulated in YSB and MM in 3D1 compared to 3D7, demonstrating that transcription
593 of this gene varies between the parents. Vacuoles play important roles in both osmotic
594 stress responses (Richards et al., 2010) and virulence (Li et al., 2021). Under salt stress the
595 vacuoles can undergo fusion and fission – changing in size and number (Richards et al.,
596 2010). *Vsp17* knockouts in *S. cerevisiae* had many small vacuoles but were resistant to
597 osmotic stress and could sporulate (Köhrer and Emr, 1993). We are unaware of any work
598 that has investigated the role of *Vsp17* in salt-stress responses of filamentous fungi.
599
600
601 **4.5. QTL reproducibility**
602 This dataset allowed us to explore the repeatability of previously identified QTL from other
603 published datasets. One earlier dataset used the same mapping populations but different
604 experimental conditions and treatments, with a different reference genome and different

genetic markers and map information (Lendenmann et al., 2015, 2014). A second earlier dataset used the same isolates and experimental conditions, but different treatments and different marker and map information (Zhong et al., 2021). Comparisons across these three data sets yielded several consistent QTL. Our analyses confirmed that a region on chromosome 11 in the 3D7x3D1 cross (Table 2, QTL No. 11) is associated with variation in melanisation and growth in multiple environments (e.g. under fungicide stress in Lendenmann et al., 2015; under oxidative stress in Zhong et al., 2021). This QTL contains the *Zmr1* transcription factor that was shown to regulate melanin production (Krishnan et al., 2018). We hypothesize that *Zmr1* also explains the variation we observed under salt-stress. A QTL associated with multiple growth and melanin traits in the 1A5x1E4 cross on chromosome 8 (Table 3, QTL No. 13) overlaps with a previously identified QTL on chromosome 8 that was associated with colony growth and tolerance to oxidative stress (Zhong et al., 2021). These findings illustrate that many of our QTL are reproducible across experiments and increases our confidence that we have identified biologically meaningful genomic regions using our automated image analyses.

CRediT authorship contribution statement

Jessica Stapley: Formal analysis, Data curation, Writing - Original Draft, Writing - Review & Editing, Resources, Data curation. Bruce A. McDonald: Conceptualization, Methodology, Writing - Review & Editing, Supervision, Project administration, Funding acquisition.

Declaration of Competing Interest

The authors declare that they have no known competing financial interests or personal relationships that could have appeared to influence the work reported in this paper

Data availability

Phenotypic and SNP data are available at ETH Data repository (DOI: 10.3929/ethz-b-000550424). All code and details of the analysis are available at (https://github.com/jessstapley/QTL-mapping-Z.-tritici).

Acknowledgments

We thank Ziming Zhong, Tiziana Valeria Vonlanthen, Bethan Turnbull, Susanne Dora, Sarah Furler, Alexandra Waltenspühl, and Jasmin Wiedmer for collecting the phenotypic data and Javier Palma-Guerrero for supervision. We thank Marcello Zala for assistance in the laboratory. This research was supported by the Swiss National Science Foundation (31003A_155955 granted to BAM).

643 **References**

644 Araújo, C.A.S., Ferreira, P.C., Pupin, B., Dias, L.P., Avalos, J., Edwards, J., Hallsworth, J.E.,
645 Rangel, D.E.N., 2020. Osmotolerance as a determinant of microbial ecology: A study
646 of phylogenetically diverse fungi. Fungal Biol. 124, 273–288.
647 https://doi.org/10.1016/j.funbio.2019.09.001
648 Badet, T., Oggenfuss, U., Abraham, L., McDonald, B.A., Croll, D., 2020. A 19-isolate
649 reference-quality global pangenome for the fungal wheat pathogen *Zymoseptoria*
650 *tritici*. BMC Biol. 18, 12. https://doi.org/10.1186/s12915-020-0744-3
651 Barbier-Brygoo, H., De Angeli, A., Filleur, S., Frachisse, J.-M., Gambale, F., Thomine, S.,
652 Wege, S., 2011. Anion channels/transporters in plants: from molecular bases to
653 regulatory networks. Annu. Rev. Plant Biol. 62, 25–51.
654 https://doi.org/10.1146/annurev-arplant-042110-103741
655 Broman, K.W., Wu, H., Sen, S., Churchill, G.A., 2003. R/qtl: QTL mapping in experimental
656 crosses. Bioinformatics 19, 889–890. https://doi.org/10.1093/bioinformatics/btg112
657 Cañero, D.C., Roncero, M.I.G., 2008. Influence of the chloride channel of *Fusarium*
658 *oxysporum* on extracellular laccase activity and virulence on tomato plants.
659 Microbiology 154, 1474–1481. https://doi.org/10.1099/mic.0.2007/015388-0
660 Croll, D., Zala, M., McDonald, B.A., 2013. Breakage-fusion-bridge Cycles and Large Insertions
661 Contribute to the Rapid Evolution of Accessory Chromosomes in a Fungal Pathogen.
662 PLOS Genet. 9, e1003567. https://doi.org/10.1371/journal.pgen.1003567
663 Dos Santos, S.C., Teixeira, M.C., Dias, P.J., Sá-Correia, I., 2014. MFS transporters required for
664 multidrug/multixenobiotic (MD/MX) resistance in the model yeast: understanding
665 their physiological function through post-genomic approaches. Front. Physiol. 5,
666 180–180. https://doi.org/10.3389/fphys.2014.00180
667 Duran, R., Cary, J.W., Calvo, A.M., 2010. Role of the Osmotic Stress Regulatory Pathway in
668 Morphogenesis and Secondary Metabolism in Filamentous Fungi. Toxins 2, 367–381.
669 https://doi.org/10.3390/toxins2040367
670 Francisco, C.S., Ma, X., Zwyssig, M.M., McDonald, B.A., Palma-Guerrero, J., 2019.
671 Morphological changes in response to environmental stresses in the fungal plant
672 pathogen *Zymoseptoria tritici*. Sci. Rep. 9, 9642. https://doi.org/10.1038/s41598-
673 019-45994-3
674 Francisco, C.S., McDonald, B.A., Palma-Guerrero, J., 2022. A transcription factor and a
675 phosphatase regulate temperature-dependent morphogenesis in a fungal plant
676 pathogen (preprint). Molecular Biology. https://doi.org/10.1101/2022.02.07.479299
677 Guo, W., Zuo, Z., Cheng, X., Sun, J., Li, H., Li, L., Qiu, J.-L., 2014. The chloride channel family
678 gene CLCd negatively regulates pathogen-associated molecular pattern (PAMP)-
679 triggered immunity in Arabidopsis. J. Exp. Bot. 65, 1205–1215.
680 https://doi.org/10.1093/jxb/ert484
681 Hohmann, S., 2002. Osmotic Stress Signaling and Osmoadaptation in Yeasts. Microbiol. Mol.
682 Biol. Rev. 66, 300–372. https://doi.org/10.1128/MMBR.66.2.300-372.2002
683 Jacob, S., Foster, A.J., Yemelin, A., Thines, E., 2015. High osmolarity glycerol (HOG) signalling
684 in *Magnaporthe oryzae*: Identification of MoYPD1 and its role in osmoregulation,
685 fungicide action, and pathogenicity. Fungal Biol. 119, 580–594.
686 https://doi.org/10.1016/j.funbio.2015.03.003
687 Jentsch, T.J., Stein, V., Weinreich, F., Zdebik, A.A., 2002. Molecular Structure and
688 Physiological Function of Chloride Channels. Physiol. Rev. 82, 503–568.
689 https://doi.org/10.1152/physrev.00029.2001

690 Jiang, C., Lv, G., Ge, J., He, B., Zhang, Z., Hu, Z., Zeng, B., 2021. Genome-wide identification
691 of the GATA transcription factor family and their expression patterns under
692 temperature and salt stress in *Aspergillus oryzae*. AMB Express 11, 56.
693 https://doi.org/10.1186/s13568-021-01212-w
694 Kogej, T., Stein, M., Volkmann, M., Gorbushina, A.A., Galinski, E.A., Gunde-Cimerman, N.,
695 2007. Osmotic adaptation of the halophilic fungus *Hortaea werneckii*: role of
696 osmolytes and melanization. Microbiology 153, 4261–4273.
697 https://doi.org/10.1099/mic.0.2007/010751-0
698 Köhrer, K., Emr, S., 1993. The yeast VPS17 gene encodes a membrane-associated protein
699 required for the sorting of soluble vacuolar hydrolases. J. Biol. Chem. 268, 559—569.
700 https://doi.org/10.1016/s0021-9258(18)54188-0
701 Krishnan, P., Meile, L., Plissonneau, C., Ma, X., Hartmann, F.E., Croll, D., McDonald, B.A.,
702 Sánchez-Vallet, A., 2018. Transposable element insertions shape gene regulation and
703 melanin production in a fungal pathogen of wheat. BMC Biol. 16, 78.
704 https://doi.org/10.1186/s12915-018-0543-2
705 Lendenmann, M.H., Croll, D., McDonald, B.A., 2015. QTL mapping of fungicide sensitivity
706 reveals novel genes and pleiotropy with melanization in the pathogen *Zymoseptoria*
707 *tritici*. Fungal Genet. Biol. 80, 53–67. https://doi.org/10.1016/j.fgb.2015.05.001
708 Lendenmann, M.H., Croll, D., Stewart, E.L., McDonald, B.A., 2014. Quantitative Trait Locus
709 Mapping of Melanization in the Plant Pathogenic Fungus *Zymoseptoria tritici*. G3
710 GenesGenomesGenetics 4, 2519–2533. https://doi.org/10.1534/g3.114.015289
711 Li, D., Qin, L., Wang, Y., Xie, Q., Li, N., Wang, S., Yuan, J., 2019. AflSte20 Regulates
712 Morphogenesis, Stress Response, and Aflatoxin Biosynthesis of *Aspergillus flavus*.
713 Toxins 11, 730. https://doi.org/10.3390/toxins11120730
714 Li, S., Zhang, S., Li, B., Li, H., 2021. The SNARE Protein CfVam7 Is Required for Growth,
715 Endoplasmic Reticulum Stress Response, and Pathogenicity of Colletotrichum
716 fructicola. Front. Microbiol. 12, 736066. https://doi.org/10.3389/fmicb.2021.736066
717 Liao, Y., Smyth, G.K., Shi, W., 2019. The R package Rsubread is easier, faster, cheaper and
718 better for alignment and quantification of RNA sequencing reads. Nucleic Acids Res.
719 47, e47–e47. https://doi.org/10.1093/nar/gkz114
720 Macovei, A., Vaid, N., Tula, S., Tuteja, N., 2012. A new DEAD-box helicase ATP-binding
721 protein (OsABP) from rice is responsive to abiotic stress. Plant Signal. Behav. 7,
722 1138–1143. https://doi.org/10.4161/psb.21343
723 Malosetti, M., van Eeuwijk, F.A., Boer, M.P., Casas, A.M., Elía, M., Moralejo, M., Bhat, P.R.,
724 Ramsay, L., Molina-Cano, J.-L., 2011. Gene and QTL detection in a three-way barley
725 cross under selection by a mixed model with kinship information using SNPs. Theor.
726 Appl. Genet. 122, 1605–1616. https://doi.org/10.1007/s00122-011-1558-z
727 Nakamura, T., Muramoto, Y., Yokota, S., Ueda, A., Takabe, T., 2004. Structural and
728 transcriptional characterization of a salt-responsive gene encoding putative ATP-
729 dependent RNA helicase in barley. Plant Sci. 167, 63–70.
730 https://doi.org/10.1016/j.plantsci.2004.03.001
731 Nguyen, L., Seok, H.-Y., Woo, D.-H., Lee, S.-Y., Moon, Y.-H., 2018. Overexpression of the
732 DEAD-Box RNA Helicase Gene AtRH17 Confers Tolerance to Salt Stress in
733 Arabidopsis. Int. J. Mol. Sci. 19, 3777. https://doi.org/10.3390/ijms19123777
734 Oddon, D.M., Diatloff, E., Roberts, S.K., 2007. A CLC chloride channel plays an essential role
735 in copper homeostasis in *Aspergillus nidulans* at increased extracellular copper

736 concentrations. Biochim. Biophys. Acta BBA - Biomembr. 1768, 2466–2477.
737 https://doi.org/10.1016/j.bbamem.2007.05.022
738 Omrane, S., Sghyer, H., Audéon, C., Lanen, C., Duplaix, C., Walker, A.-S., Fillinger, S., 2015.
739 Fungicide efflux and the MgMFS1 transporter contribute to the multidrug resistance
740 phenotype in *Z ymoseptoria tritici* field isolates: Fungicide efflux & *MgMFS 1*
741 contribute to MDR in *Z. tritici*. Environ. Microbiol. 17, 2805–2823.
742 https://doi.org/10.1111/1462-2920.12781
743 Palma-Guerrero, J., Ma, X., Torriani, S.F.F., Zala, M., Francisco, C.S., Hartmann, F.E., Croll, D.,
744 McDonald, B.A., 2017. Comparative Transcriptome Analyses in *Zymoseptoria tritici*
745 Reveal Significant Differences in Gene Expression Among Strains During Plant
746 Infection. Mol. Plant-Microbe Interactions® 30, 231–244.
747 https://doi.org/10.1094/MPMI-07-16-0146-R
748 Pandey, S., Prasad, A., Sharma, N., Prasad, M., 2020. Linking the plant stress responses with
749 RNA helicases. Plant Sci. 299, 110607.
750 https://doi.org/10.1016/j.plantsci.2020.110607
751 Plissonneau, C., Hartmann, F.E., Croll, D., 2018. Pangenome analyses of the wheat pathogen
752 *Zymoseptoria tritici* reveal the structural basis of a highly plastic eukaryotic genome.
753 BMC Biol. 16, 5. https://doi.org/10.1186/s12915-017-0457-4
754 Plissonneau, C., Stürchler, A., Croll, D., 2016. The Evolution of Orphan Regions in Genomes
755 of a Fungal Pathogen of Wheat. mBio 7. https://doi.org/10.1128/mBio.01231-16
756 R Core Team, 2020. R: A language and environment for statistical computing.
757 Richards, A., Veses, V., Gow, N.A.R., 2010. Vacuole dynamics in fungi. Fungal Biol. Rev. 24,
758 93–105. https://doi.org/10.1016/j.fbr.2010.04.002
759 Robinson, M.D., McCarthy, D.J., Smyth, G.K., 2010. edgeR: a Bioconductor package for
760 differential expression analysis of digital gene expression data. Bioinformatics 26,
761 139–140. https://doi.org/10.1093/bioinformatics/btp616
762 RStudio Team, 2020. RStudio: Integrated Development Environment for R.
763 Shi, D., Ren, W., Wang, J., Zhang, J., Mbadianya, J.I., Mao, X., Chen, C., 2021. The
764 transcription factor FgNsf1 regulates fungal development, virulence and stress
765 responses in Fusarium graminearum. J. Integr. Agric. 20, 2156–2169.
766 https://doi.org/10.1016/S2095-3119(20)63339-1
767 Son, H., Park, A.R., Lim, J.Y., Lee, Y.-W., 2015. Fss1 is involved in the regulation of an *ENA5*
768 homologue for sodium and lithium tolerance in *F usarium graminearum*: Roles of
769 Fss1 in *Fusarium graminearum*. Environ. Microbiol. 17, 2048–2063.
770 https://doi.org/10.1111/1462-2920.12757
771 Zhan, J., Linde, C.C., Jurgens, T., Merz, U., Steinebrunner, F., McDONALD, B.A., 2005.
772 Variation for neutral markers is correlated with variation for quantitative traits in the
773 plant pathogenic fungus Mycosphaerella graminicola. Mol. Ecol. 14, 2683–2693.
774 https://doi.org/10.1111/j.1365-294X.2005.02638.x
775 Zhang, X., Zhao, X., Feng, C., Liu, N., Feng, H., Wang, X., Mu, X., Huang, L., Kang, Z., 2014. The
776 cloning and characterization of a DEAD-Box RNA helicase from stress-responsive
777 wheat. Physiol. Mol. Plant Pathol. 88, 36–42.
778 https://doi.org/10.1016/j.pmpp.2014.07.004
779 Zhong, Z., Marcel, T.C., Hartmann, F.E., Ma, X., Plissonneau, C., Zala, M., Ducasse, A.,
780 Confais, J., Compain, J., Lapalu, N., Amselem, J., McDonald, B.A., Croll, D., Palma-
781 Guerrero, J., 2017. A small secreted protein in *Zymoseptoria tritici* is responsible for

782 avirulence on wheat cultivars carrying the Stb6 resistance gene. New Phytol. 214,
783 619–631. https://doi.org/10.1111/nph.14434
784 Zhong, Z., McDonald, B.A., Palma-Guerrero, J., 2021. Tolerance to oxidative stress is
785 associated with both oxidative stress response and inherent growth in a fungal
786 wheat pathogen. Genetics 217, iyaa022. https://doi.org/10.1093/genetics/iyaa022
787 Zhu, X., Williamson, P.R., 2003. A CLC-type chloride channel gene is required for laccase
788 activity and virulence in *Cryptococcus neoformans*: CLC-A of *Cryptococcus*
789 *neoformans*. Mol. Microbiol. 50, 1271–1281. https://doi.org/10.1046/j.1365-
790 2958.2003.03752.x
791

792

Figure 1. Trait variation in the control and salt stress environments across offspring in each cross. Top panel: Points are mean colony radius in the control and KCl environment at 8 and 12 dpi, smoothed lines demonstrate linear change over time. Middle panel: Points are mean grey value in the control and KCL environments at 8 and 12 dpi, smoothed lines demonstrate linear change over time. Bottom panel: Growth rate KCl tolerance and melanisation rate KCl tolerance (KCl tolerance = rate in KCl/rate in control conditions, see section 2.4) between the two crosses.

Figure 2. LOD plots from interval mapping for representative traits a) growth rate and b) melanisation rate in the control environment (grey) and in the KCl environment (orange) in the 3D7x3D1 cross. Each sub-panel is a chromosome with the chromosome number indicated at the top. Some numbers are missing because *Zymoseptoria tritici* carries eight accessory chromosomes (Chr 14-21) that show presence/absence polymorphisms among isolates. The dashed horizontal lines indicate the LOD significance thresholds for each trait based on permutation. The numbers above the QTL peaks correspond to the QTL numbers from Table 2. For LOD plots of all traits see Supplementary Information (S2).

Figure 3. LOD plots from interval mapping for representative traits a) growth rate and b) melanisation rate in the control environment (grey) and in the KCl environment (orange) in the 1A5x1E4 cross. Some numbers are missing because *Zymoseptoria tritici* carries eight accessory chromosomes (Chr 14-21) that show presence/absence polymorphisms among isolates. The dashed horizontal lines indicate the LOD significance thresholds for each trait based on permutation. The numbers above the QTL peaks correspond to the QTL numbers from Table 3. For LOD plots of all traits see Supplementary Information (S3) .

Figure 4. QTL on Chromosome 3 for three traits related to growth under osmotic stress in the 3D7x3D1 cross. The three traits were colony radius at 8 dpi, colony radius KCl tolerance at 8 and 12 dpi (KCl tolerance = colony radius in KCl/colony radius in control conditions , see section 2.4). a) LOD peak and Bayes credible interval (shaded) from interval mapping, with SNP positions indicated on the x-axis as black vertical lines, b) Alignment of the 36 genes within the QTL interval between the 3D7 and 3D1 parental strains – orange-coloured genes are the six most promising candidate genes described in the main text and c) allelic effects

825 of 94 SNPs within the QTL interval on mean colony radius in KCl at 8 dpi. Isolates carrying
826 the reference allele (ref=3D7) shown in grey have smaller colonies compared to the
827 alternative allele (alt=3D1) shown in orange. SNP position in base pairs is shown on the x-
828 axis. The marker with the highest LOD is at position 737773 bp.
829
830 Supplementary Material
831 S1. Summary of genetic linkage maps.
832 S2. Plots of phenotypic correlations.
833 S3. LOD plots from interval mapping for all traits in the 3D7x3D1 cross.
834 S4. LOD plots from interval mapping for all traits in the 1A5x1E4 cross.

Table 1. Summary of the QTL mapping results for all traits. Grey value and colony radius were measured at two time points: 8 and 12 dpi. Growth rate was measured as the change in colony radius/number of days(4). Melanisation rate was measured as the change in grey value/number of days(4). Colony radius/grey value KCl tolerance were calculated by dividing the value (grey value or colony radius) in the control environment by the value in the KCl environment. Growth rate/Melanisation KCl tolerance were calculated by dividing the rate (melanisation or growth) in the control environment by the rate in the KCl environment. The QTL peak columns show the chromosomal position of significant QTL peak for each trait in the 3D7x3D1 and 1A5x1E4 crosses respectively, and the final column contained estimated heritability (h^2) for each trait.

Data Type	Environment	DPI	Measurement	Measurement	QTL peak 3D7x3D1	h^2	QTL peak 1A5x1E4	h^2
Time point	Control	8	Colony radius	Colony radius in Control at 8dpi	3,8,10,11	0.53	2,3,8	0.56
Time point	Control	12	Colony radius	Colony radius in Control at 12dpi	3,7,8,10,11	0.62	7,8	0.48
Time point	KCl	8	Colony radius	Colony radius in KCl at 8dpi	3,4	0.64	6,	0.5
Time point	KCl	12	Colony radius	Colony radius in KCl at 12dpi	3,8	0.6	1,8	0.52
Time point	Control	8	Grey value	Grey value in Control at 8dpi	8,10,11	0.42	1,2,3,8	0.63
Time point	Control	12	Grey value	Grey value in Control at 12dpi	11	0.22	2,3,8	0.44
Time point	KCl	8	Grey value	Grey value in KCl at 8dpi	8,11	0.54	8	0.34
Time point	KCl	12	Grey value	Grey value in KCl at 12dpi	1,2,11	0.34	No Sig. QTL	0.29
Rate	Control	8-12	Growth rate	Growth rate in Control	3,8,11	0.61	7,8	0.33
Rate	KCl	8-12	Growth rate	Growth rate in KCl	3,8,11	0.45	8,	0.49
Rate	Control	8-12	Melanisation rate	Melanisation rate in Control	10	0.28	2,3,12	0.54
Rate	KCl	8-12	Melanisation rate	Melanisation rate in KCl	1,6	0.32	No Sig. QTL	0.27
Tolerance	Both	8	Grey value	Grey value KCl tolerance at 8 dpi	8,10	0.37	1,2,3,8	0.58
Tolerance	Both	12	Grey value	Grey value KCl tolerance at 12 dpi	11	0.18	No Sig. QTL	0.34
Tolerance	Both	8	Colony radius	Colony radius KCl tolerance at 8dpi	3,4,10	0.59	8	0.42
Tolerance	Both	12	Colony radius	Colony radius KCl tolerance at 12dpi	3,10,11	0.47	1	0.37
Tolerance	Both	8-12	Growth rate	Growth rate KCl tolerance	11	0.4	1,5	0.45
Tolerance	Both	8-12	Melanisation rate	Melanisation rate KCl tolerance	No Sig. QTL	0.14	1	0.32

Table 2. Description of all QTL identified from the 3D7x3D1 cross, including map and physical position of the LOD peak marker, the bayes credible interval length and the number of genes within the interval. PVE is the proportion of variance explained by the QTL. QTL number is a number assigned to a particular QTL peak which groups overlapping QTLs.

Type	Chr	Pos (cM)	LOD	Pos (bp)	No. markers	Interval Start (bp)	Interval end (bp)	Interval size (bp)	No. Genes	PVE	QTL number
Melanisation rate in KCl	1	457.43	6.18	1590235	2915	1035571	2769729	1734.158	598	0.10	1
Melanisation rate KCl tolerance	1	540.00	3.40	2295356	9000	788430	6389989	5601.559	1977	0.06	1
Grey value in KCl at 12dpi	1	576.00	5.99	2717234	519	2295128	2769729	474.601	174	0.10	1
Grey value in KCl at 12dpi	2	261.00	5.07	691536	141	679366	711981	32.615	15	0.09	2
Colony radius KCl tolerance at 12dpi	3	142.92	4.49	719549	553	396401	944712	548.311	125	0.08	3
Colony radius KCl tolerance at 8dpi	3	144.00	14.62	737773	105	588483	751983	163.5	36	0.23	3
Colony radius in KCl at 8dpi	3	144.15	22.83	737773	94	588483	737773	149.29	31	0.33	3
Growth rate in Control	3	415.00	5.31	2537296	2204	1982744	3347765	1365.021	462	0.09	4
Colony radius in Control at 12dpi	3	456.63	8.11	2993469	427	2971359	3196103	224.744	79	0.13	4
Colony radius in Control at 8dpi	3	482.67	7.09	3056536	428	2982086	3199430	217.344	76	0.12	4
Growth rate in KCl	3	485.65	4.93	3110053	845	2971359	3347765	376.406	132	0.08	4
Colony radius in KCl at 12dpi	3	485.65	4.99	3110053	3084	516017	3203947	2687.93	813	0.08	4
Colony radius KCl tolerance at 8dpi	4	400.00	4.28	1936846	1000	1845763	2448166	602.403	200	0.07	5
Colony radius in KCl at 8dpi	4	403.76	4.37	2013908	986	1867509	2448166	580.657	194	0.07	5
Melanisation rate in KCl	6	220.14	6.24	1767543	479	1568163	1981193	413.03	124	0.10	6
Colony radius in Control at 12dpi	7	186.78	4.47	1109088	1366	511101	1377451	866.35	265	0.08	7
Grey value in KCl at 8dpi	8	680.87	5.69	943669	732	502305	974947	472.642	123	0.10	8
Growth rate in Control	8	746.72	7.31	1100862	542	1071962	1221280	149.318	65	0.12	9
Colony radius in Control at 12dpi	8	746.72	10.77	1100862	274	1091579	1164224	72.645	29	0.17	9
Growth rate in KCl	8	747.72	9.66	1100862	667	1091692	1284370	192.678	77	0.16	9
Colony radius in KCl at 12dpi	8	751.61	9.79	1112633	670	1100862	1292397	191.535	76	0.16	9
Colony radius in Control at 8dpi	8	765.72	8.04	1221337	751	1091475	1354349	262.874	108	0.13	9
Grey value KCl tolerance at 8dpi	8	776.11	4.22	1350673	2608	962119	2165894	1203.775	457	0.07	9

Grey value in Control at 8dpi	8	776.11	4.35	1350706	2549	981398	2175005	1193.607	450	0.07	9
Grey value in Control at 8dpi	10	199.98	12.37	775475	160	769669	861699	92.03	32	0.20	10
Grey value KCl tolerance at 8dpi	10	199.98	10.68	775475	281	769669	919978	150.309	56	0.17	10
Melanisation rate in KCl	10	200.35	8.66	792011	299	769669	924425	154.756	59	0.14	10
Colony radius in Control at 8dpi	10	200.72	12.32	792272	299	769669	924425	154.756	59	0.19	10
Colony radius KCl tolerance at 8dpi	10	211.51	10.58	924412	283	792019	924425	132.406	53	0.17	10
Colony radius KCl tolerance at 12dpi	10	211.51	6.68	924414	1081	749521	1302645	553.124	211	0.11	10
Colony radius in Control at 12dpi	10	212.61	4.92	924425	540	749521	1054575	305.054	116	0.08	10
Colony radius in Control at 8dpi	11	183.07	4.20	507361	528	311631	698718	387.087	128	0.07	11
Colony radius KCl tolerance at 12dpi	11	188.28	5.60	581439	1340	74200	890544	816.344	268	0.09	11
Grey value in KCl at 12dpi	11	192.28	6.87	605810	408	463714	776764	313.05	99	0.11	11
Growth rate in Control	11	193.00	19.63	616039	5	616039	658119	42.08	13	0.29	11
Growth rate in KCl	11	193.00	5.47	616039	219	468760	698718	229.958	72	0.09	11
Colony radius in Control at 12dpi	11	193.00	16.79	616039	25	601600	658119	56.519	16	0.26	11
Grey value in Control at 12dpi	11	194.11	6.64	657530	498	514049	870059	356.01	121	0.11	11
Grey value KCl tolerance at 12dpi	11	194.11	5.55	657530	700	367519	870059	502.54	168	0.09	11
Grey value in Control at 8dpi	11	194.11	5.30	658070	244	463714	704331	240.617	77	0.09	11
Grey value in KCl at 8dpi	11	194.11	17.09	658119	5	616039	658119	42.08	13	0.26	11
Growth rate KCl tolerance	11	195.28	7.45	658119	370	500942	802650	301.708	98	0.12	11

Table 3. Description of all QTLs identified from the 1A5x1E4 cross, including map and physical position of the LOD peak marker, the bayes credible interval length and the number of genes within the interval. PVE is the proportion of variance explained by the QTL. QTL number is a number assigned to a particular QTL peak which identifies overlapping QTLs..

Type	Chr	Pos (cM)	LOD	Pos (bp)	No. markers	Interval Start (bp)	Interval end (bp)	Interval size (bp)	No. Genes	PVE	QTL number
Grey value in Control at 8dpi	1	328.91	5.69	572065	402	442697	727696	284.999	92	0.10	1
Grey value KCl tolerance at 8dpi	1	328.91	5.01	572065	405	442697	732023	289.326	93	0.08	1
Melanisation rate KCl tolerance	1	328.91	4.46	572065	463	461577	779936	318.359	102	0.08	1
Colony radius KCl tolerance at 12dpi	1	559.12	4.07	1849200	4654	399579	5725682	5326.103	1964	0.07	2
Growth rate KCl tolerance	1	797.00	4.80	3405315	3068	399544	3488556	3089.012	1151	0.08	3
Colony radius in KCl at 12dpi	1	1104.00	4.03	5792644	4774	372886	5956797	5583.911	2056	0.07	4
Melanisation rate in Control	2	70.00	6.56	574965	1211	405115	1914465	1509.35	509	0.11	5
Grey value in Control at 12dpi	2	204.66	4.55	1438934	618	1284536	2152463	867.927	281	0.08	6
Grey value in Control at 8dpi	2	204.66	18.08	1438934	185	1438863	1748215	309.352	95	0.27	6
Grey value KCl tolerance at 8dpi	2	204.66	15.97	1438934	184	1438934	1748215	309.281	95	0.24	6
Colony radius in Control at 8dpi	2	211.42	8.76	1631840	217	1438934	1776132	337.198	105	0.14	6
Grey value KCl tolerance at 8dpi	3	147.00	6.15	1325440	210	1243932	1684531	440.599	179	0.10	7
Grey value in Control at 8dpi	3	148.00	6.66	1325440	133	1325422	1592801	267.379	115	0.11	7
Colony radius in Control at 8dpi	3	163.74	5.83	1521535	725	355042	1592801	1237.759	374	0.10	8
Melanisation rate in Control	3	193.38	11.99	1711037	290	1489966	2105601	615.635	180	0.19	9
Grey value in Control at 12dpi	3	198.73	4.04	1928783	860	1743111	2927356	1184.245	361	0.07	9
Growth rate KCl tolerance	5	399.00	4.34	2638913	155	2511016	2658480	147.464	48	0.07	10
Colony radius in KCl at 8dpi	6	179.00	4.48	1512508	594	778583	1557528	778.945	256	0.08	11
Growth rate in Control	7	158.82	4.43	539824	255	437699	651318	213.619	80	0.07	12
Colony radius in Control at 12dpi	7	158.82	4.67	539837	254	437718	651318	213.6	80	0.08	12
Growth rate in KCl	8	76.80	8.79	274792	82	256529	346224	89.695	25	0.14	13
Colony radius in KCl at 12dpi	8	76.80	8.94	274792	67	256529	313758	57.229	17	0.15	13
Grey value in Control at 12dpi	8	78.58	4.92	302772	882	89684	921404	831.72	308	0.08	13

Grey value in Control at 8dpi	8	79.00	12.12	302772	66	270834	346224	75.39	22	0.19	13
Colony radius in Control at 12dpi	8	79.00	9.72	302772	80	260355	346224	85.869	24	0.16	13
Colony radius in Control at 8dpi	8	79.00	11.06	302772	415	260101	732444	472.343	163	0.18	13
Grey value KCl tolerance at 8dpi	8	79.00	8.26	302772	339	89573	346224	256.651	90	0.14	13
Colony radius KCl tolerance at 8dpi	8	137.00	5.05	832180	1177	589084	1648406	1059.322	396	0.08	13
Grey value in KCl at 8dpi	8	164.00	4.33	1377926	1406	305075	1623437	1318.362	485	0.07	13
Melanisation rate in Control	12	126.74	4.24	473688	275	441706	821603	379.897	101	0.07	14

Table 4 Genes within the QTL interval for colony radius at 8 dpi in KCl and colony radius KCl tolerance at 8 dpi in the 3D7x3D1 cross. Bold indicates genes that are the most promising candidate genes, as described in the main text. Gene sequence similarity between the two parental strains was obtained using BLAST. DGE: Differential gene expression column indicates if the gene was differentially expressed between parents in any one of the data sets used (in planta or in vitro, see Methods in main text). The annotations were obtained using Interproscan using multiple protein databases, here we show only the PFAM annotation.

Chr	Gene id 3D7	Gene start	Gene end	Gene id 3D1	Sequence similarity (%)	DGE	**Annotation**
3	**ZT3D7_G3622**	**598091**	**599743**	**ZT3D1_G3567**	**97.68**	**yes**	**Fungal-specific transcription factor domain**
3	ZT3D7_G3623	637954	638542	ZT3D1_G7387	96.23	NA	
3	ZT3D7_G3624	653468	654397	ZT3D1_G3569	90.78	yes	Protein of unknown function (DUF1349)
3	ZT3D7_G3625	655237	656628	ZT3D1_G3570	97.04	yes	
3	ZT3D7_G3626	667030	667567	NA		yes	Pterin 4 alpha carbinolamine dehydratase
3	ZT3D7_G3627	667812	668321	ZT3D1_G3571	98.46	yes	
3	ZT3D7_G3628	670445	671787	ZT3D1_G3572	100.00	yes	Transketolase, pyrimidine binding domain, Transketolase, C-terminal domain
3	ZT3D7_G3629	672336	673658	ZT3D1_G3573	99.83	NA	
3	ZT3D7_G3630	674777	676658	ZT3D1_G3574	99.96	yes	Dehydratase family
3	ZT3D7_G3631	677782	680135	ZT3D1_G3576	97.72	yes	ABC transporter, ABC transporter
3	ZT3D7_G3632	680734	681942	ZT3D1_G3577	97.73	yes	Epoxide hydrolase N terminus
3	ZT3D7_G3633	683647	685131	ZT3D1_G3578	81.12	NA	Phosphotransferase enzyme family
3	ZT3D7_G3634	685575	685937	ZT3D1_G3579	98.96	yes	
3	**ZT3D7_G3635**	**686721**	**692363**	**ZT3D1_G3580**	**99.07**	**yes**	**Protein kinase domain, Protein kinase C terminal domain, N-terminal half of MaoC dehydratase, MaoC like domain, C2 domain**
3	ZT3D7_G3636	693114	696535	ZT3D1_G3582	99.50	yes	Importin-beta N-terminal domain, Cse1
3	**ZT3D7_G3637**	**697014**	**700871**	**ZT3D1_G3583**	**97.44**	**yes**	**DEAD/DEAH box helicase, rRNA-processing arch domain, DSHCT (NUC185) domain, Ski2 N-terminal region, Helicase conserved C-terminal domain**
3	ZT3D7_G3638	701182	702047	ZT3D1_G3584	98.74	yes	short chain dehydrogenase
3	**ZT3D7_G3639**	**702431**	**704143**	**ZT3D1_G3585**	**97.16**	**yes**	**Major Facilitator Superfamily**
3	ZT3D7_G3640	705425	706303	ZT3D1_G3587	99.91	yes	
3	ZT3D7_G3641	706740	707975	ZT3D1_G3588	98.53	yes	
3	ZT3D7_G3642	708779	709336	ZT3D1_G3589	98.33	NS	
3	ZT3D7_G3643	709874	711886	ZT3D1_G3590	94.46	yes	Ubiquitin-conjugating enzyme
3	ZT3D7_G3644	712327	715212	ZT3D1_G3591	98.93	yes	Utp14 protein
3	ZT3D7_G3645	715430	715798	ZT3D1_G3592	99.74	no	Mitochondrial ribosomal protein L27

3	ZT3D7_G3646	716302	720497	ZT3D1_G3593	98.96	NA	Staphylococcal nuclease homologue, short chain dehydrogenase, Enoyl-(Acyl carrier protein) reductase, Tudor domain
3	ZT3D7_G3647	720900	723737	ZT3D1_G3594	99.38	yes	PQQ-like domain, ER membrane protein complex subunit 1, C-terminal
3	ZT3D7_G3648	725571	726437	ZT3D1_G3595	99.02	no	Ras family
3	ZT3D7_G3649	726651	727599	NA		yes	NmrA-like family
3	ZT3D7_G3650	727935	729979	ZT3D1_G3596	98.53	no	Heterokaryon incompatibility protein (HET)
3	ZT3D7_G3651	730698	731819	ZT3D1_G3597	99.93	yes	Transaldolase/Fructose-6-phosphate aldolase
3	ZT3D7_G3652	732329	733083	ZT3D1_G3598	96.53	yes	Copper/zinc superoxide dismutase (SODC)
3	ZT3D7_G3653	734230	736078	ZT3D1_G3599	99.73	yes	FGGY family of carbohydrate kinases, C-terminal domain, FGGY family of carbohydrate kinases, N-terminal domain
3	ZT3D7_G3654	737260	737987	ZT3D1_G3600	99.87	yes	
3	**ZT3D7_G3655**	**739211**	**741757**	**ZT3D1_G3601**	**99.97**	**yes**	**CBS domain, Voltage gated chloride channel**
3	ZT3D7_G3656	743352	744442	ZT3D1_G3602	99.73	yes	Protein of unknown function (DUF1295)
3	ZT3D7_G3657	744744	746896	ZT3D1_G3603	99.92	yes	Pro-kumamolisin, activation domain
3	**ZT3D7_G3658**	**748505**	**750639**	**ZT3D1_G3604**	**100**	**yes**	**PX domain, Vps5 C terminal like**

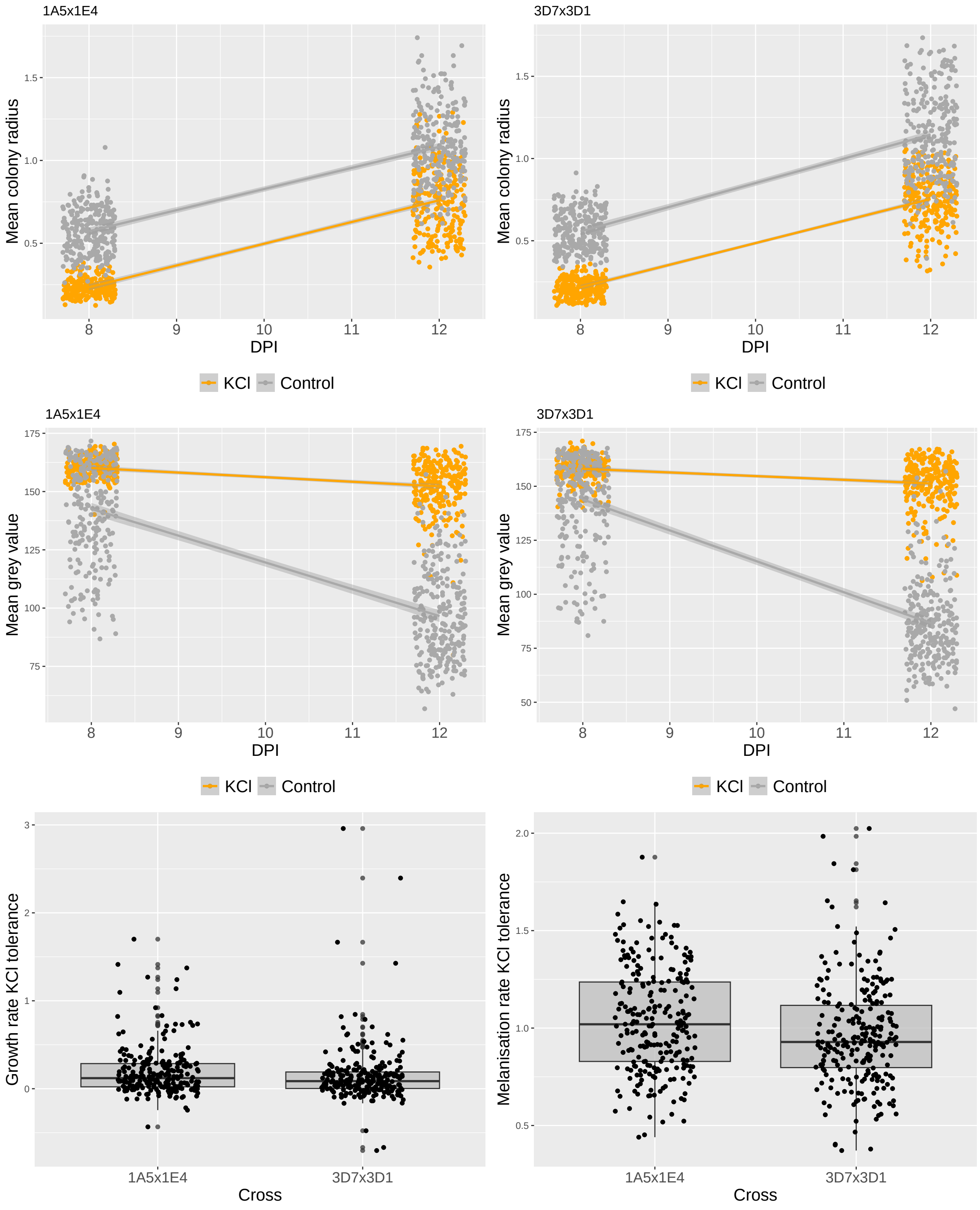
1A5x1E4
3D7x3D1
Mean colony radius
1.5
1.0
0.5
8
9
10
11
12
DPI
KCl
Control
Mean grey value
175
150
125
100
75
50
Growth rate KCl tolerance
3
2
1
0
Melanisation rate KCl tolerance
2.0
1.5
1.0
0.5
Cross

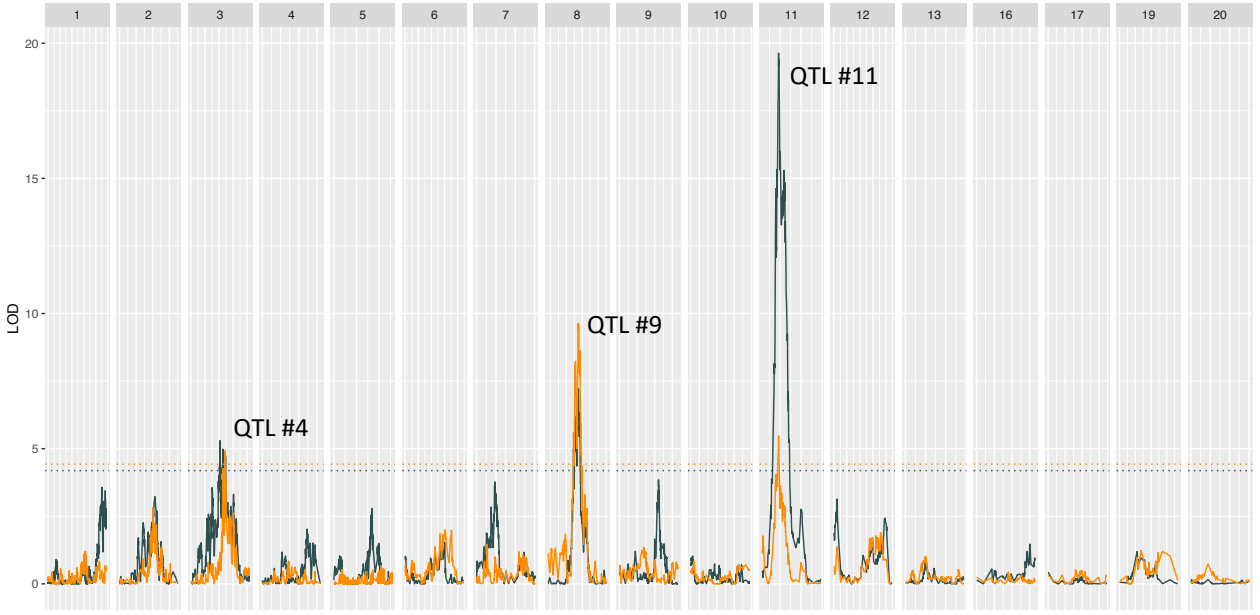

Growth rate — Control — KCl

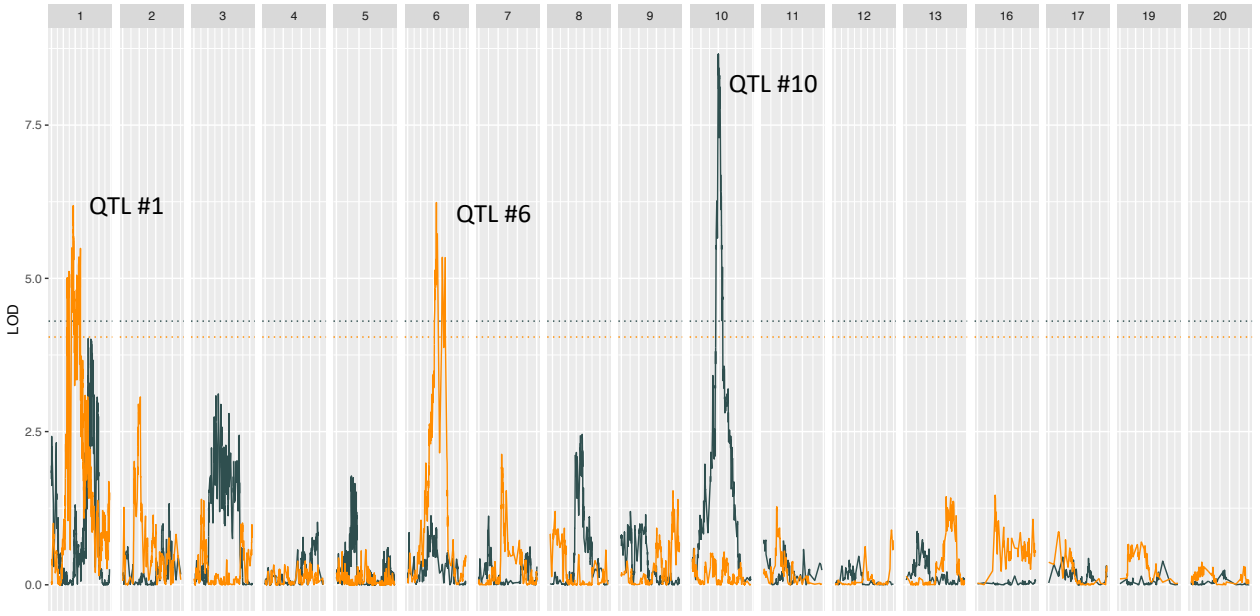

Melanisation rate — Control — KCl

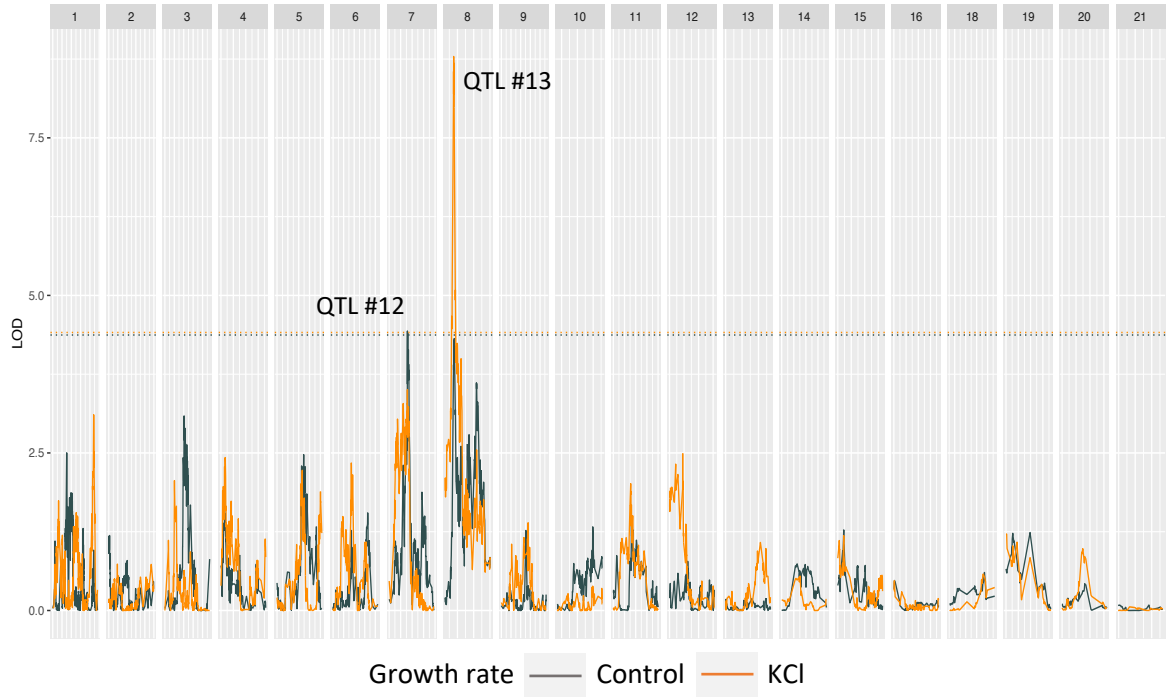
1
2
3
4
5
6
7
8
9
10
11
12
13
14
15
16
18
19
20
21
QTL #13
QTL #12
LOD
7.5
5.0
2.5
0.0
Growth rate
Control
KCl

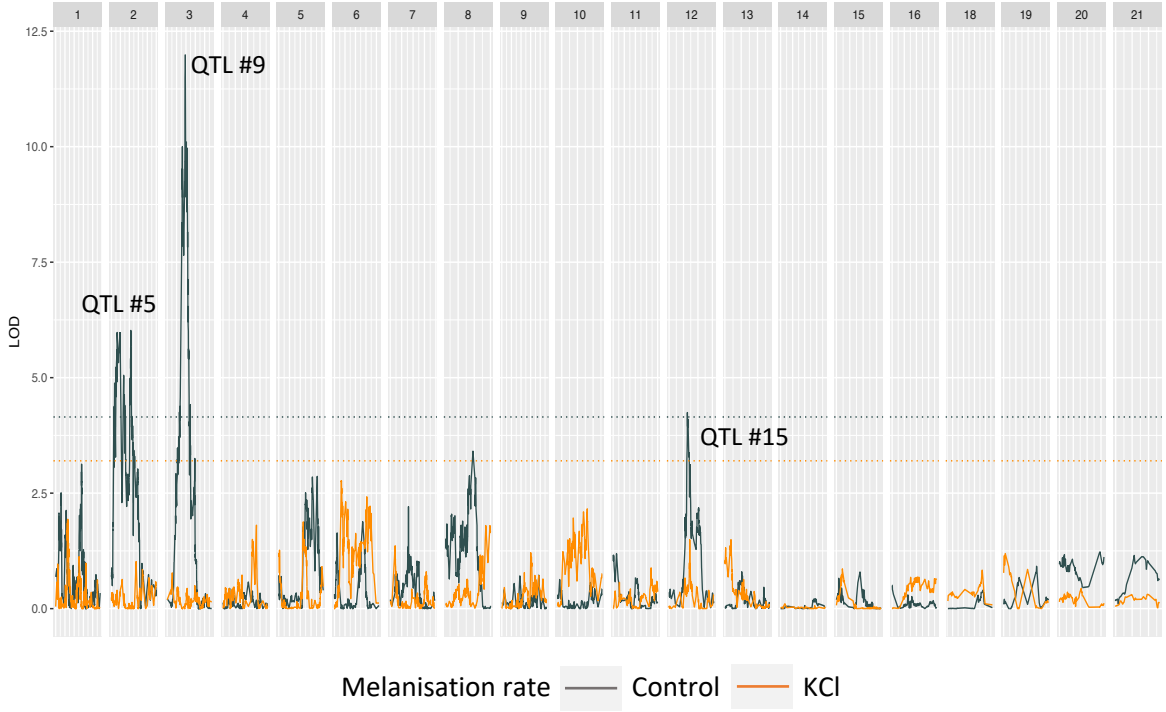
1
2
3
4
5
6
7
8
9
10
11
12
13
14
15
16
18
19
20
21
QTL #9
QTL #5
QTL #15
LOD
12.5
10.0
7.5
5.0
2.5
0.0
Melanisation rate
Control
KCl

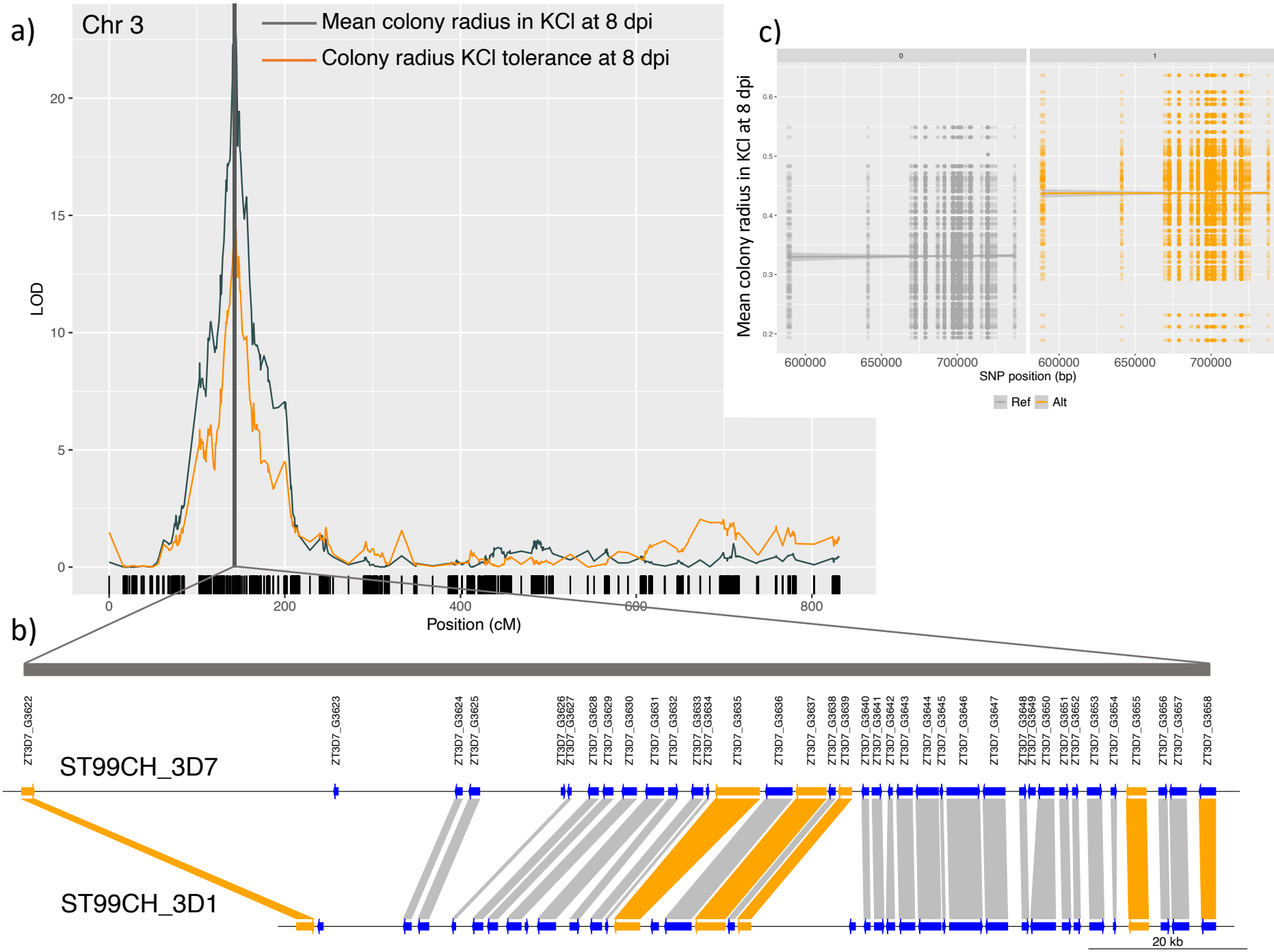
a)
Chr 3
Mean colony radius in KCl at 8 dpi
Colony radius KCl tolerance at 8 dpi
LOD
Position (cM)
c)
Mean colony radius in KCl at 8 dpi
SNP position (bp)
Ref
Alt
b)
ST99CH_3D7
ST99CH_3D1
20 kb